

Gaseous CO Abundance—An Evolutionary Tracer for Molecular Clouds

Tie Liu¹, Yuefang Wu¹, Huawei Zhang¹

Received _____; accepted _____

Accepted to ApJL

¹Department of Astronomy, Peking University, 100871, Beijing China; liutiepku@gmail.com, ywu@pku.edu.cn

ABSTRACT

Planck cold clumps are among the most promising objects to investigate the initial conditions of the evolution of molecular clouds. In this work, by combining the dust emission data from the survey of Planck satellite with the molecular data of $^{12}\text{CO}/^{13}\text{CO}$ (1-0) lines from observations with the Purple Mountain Observatory (PMO) 13.7 m telescope, we investigate the CO abundance, CO depletion and CO-to- H_2 conversion factor of 674 clumps in the early cold cores (ECC) sample. The median and mean values of the CO abundance are 0.89×10^{-4} and 1.28×10^{-4} , respectively. The mean and median of CO depletion factor are 1.7 and 0.9, respectively. The median value of $X_{\text{CO-to-H}_2}$ for the whole sample is $2.8 \times 10^{20} \text{ cm}^{-2} \text{ K}^{-1} \text{ km}^{-1} \text{ s}$. The CO abundance, CO depletion factor and CO-to- H_2 conversion factor are strongly (anti-)correlated to other physical parameters (e.g. dust temperature, dust emissivity spectral index, column density, volume density and luminosity-to-mass ratio). To conclude, the gaseous CO abundance can be used as an evolutionary tracer for molecular clouds.

Subject headings: ISM: abundances — ISM: clouds — ISM: evolution — ISM: molecules

1. Introduction

Carbon monoxide (CO) is the second most abundant molecular species (after H₂) in molecular clouds and is often used to determine the column density of molecular hydrogen by assuming a [CO/H₂] abundance ratio. Previously different authors used different [CO/H₂] abundance ratio (Wu et al. 2004), which is from 2.5×10^{-5} (Rodríguez et al. 1982) to 10^{-4} (Garden et al. 1991). In addition, the observations of ¹²CO (1-0) are often used to estimate the molecular content of entire galaxies by applying an empirical CO-to-H₂ conversion factor ($X_{CO-to-H_2} = N_{H_2}/I_{CO}$), which is $(1.8 \pm 0.3) \times 10^{20} \text{ cm}^{-2} \text{ K}^{-1} \text{ km}^{-1} \text{ s}$ for the disk of the Milky Way (Dame, Hartmann & Thaddeus 2001). However, the CO-to-H₂ conversion factor varies with different methods used in measuring the column density of H₂ (Pineda, Caselli & Goodman 2008). The reliability of using CO as a tracer for molecular mass should be taken seriously because the abundance of gaseous CO is very sensitive to chemical effects such as CO depletion in cold regions.

Towards five low-mass starless cores, Tafalla et al. (2002) found that the abundance of CO near the core center decreases by at least 1 or 2 orders of magnitude with respect to the value in the outer core, indicating that huge amount of gaseous CO freezes out onto dust grains in the dense region. In the observations towards 21 IRDCs, the CO depletion factor (f_D), which is defined as the ratio of expected standard gas phase CO abundance to the observed CO abundance, is in between 5 and 78, with a median value of 29 (Fontani et al. 2012). Additionally, the depletion of gas-phase CO seems to increase with density. Caselli et al. (1999) found that the depletion factor is up to ~ 10 where the mass surface density is $\Sigma \simeq 0.6 \text{ g cm}^{-2}$, while Kramer et al. (1999) found the depletion factor is ~ 2.5 for regions with $\Sigma \simeq 0.1 - 0.15 \text{ g cm}^{-2}$. In the observations towards the filamentary IRDC G035.30-00.33, Hernandez et al. (2011) found the depletion factor increases by about a factor of five as Σ increases from ~ 0.02 to $\sim 0.2 \text{ g cm}^{-2}$. By combining data from the Five College Radio Astronomy Observatory CO Mapping Survey of the Taurus molecular cloud with extinction data for a sample of 292 background field stars, Whittet, Goldsmith & Pineda (2010)

found that the mean ratio of icy CO to gaseous CO increases monotonically from negligible levels for visual extinctions $A_V \leq 5$ to ~ 0.3 at $A_V = 10$ and ~ 0.6 at $A_V = 30$. However, in the survey towards the Gould Belt clouds, only in the cases of starless cores in Taurus and protostellar cores in Serpens, there is a correlation between the column densities of the cores and the depletion factor (Christie et al. 2012). And similarly, CO depletion factor does not seem to be correlated to any other physical parameter in the observations towards 21 IRDCs (Fontani et al. 2012).

However, previous works are severely subject to relatively small sample and thus they can not statistically investigate the relationships between gaseous CO abundance and the other physical parameters. In this paper, we use the early cold cores (ECC) sample to systemically investigate the gaseous CO abundance, CO depletion and CO-to-H₂ conversion factor in molecular clumps. Our results suggest that the gaseous CO abundance strongly (anti-)correlates with dust temperature, dust emissivity spectral index, column density, volume density and luminosity-to-mass ratio.

2. Data

The early cold cores (ECC) sample is a subset of the Planck Early Release Compact Source Catalogue and contains only the most reliable detections (SNR>15) of sources with color temperature below 14 K (Planck Collaboration. et al. 2011). In the ECC, the photometry is carried out on the original Planck maps by placing an aperture of 5' radius on top of the detection (Planck Collaboration. et al. 2011). The background is estimated using an annulus around the aperture with an inner radius of 5' and an outer radius of 10'. Temperatures and dust emissivity spectral indexes are derived from a fit to all four bands (IRIS 3 THz and Planck 857, 545 and 353 GHz) (Planck Collaboration. et al. 2011). The major and minor axis of each source are also obtained from ellipse fit (Planck Collaboration. et al. 2011). We extracted the aperture flux density at 857 GHz, the core temperature, core emissivity index as well as the ellipse major and minor axis of each clump from the ECC catalogue.

We have carried out a follow-up observations towards 674 ECC clumps with the Purple Mountain Observatory (PMO) 13.7 m telescope. The details of the observations can be found in Wu et al. (2012). The half-power beam width of the telescope at the 115 GHz frequency band is 56". The main beam efficiency is ~50%. For each identified ^{13}CO (1-0) component, their kinematic distance and galactocentric distance were calculated (Wu et al. 2012).

3. Results

3.1. Abundance of gaseous ^{12}CO

The excitation temperature of ^{12}CO (1-0) can be derived as following (Garden et al. 1991):

$$T_r = \frac{T_a^*}{\eta_b} = \frac{h\nu}{k} \left[\frac{1}{\exp(h\nu/kT_{ex}) - 1} - \frac{1}{\exp(h\nu/kT_{bg}) - 1} \right] \times [1 - \exp(-\tau)] f \quad (1)$$

here T_a^* is the antenna temperature, and T_r is the brightness temperature corrected with beam efficiency η_b , h is the Planck constant, k is the Boltzmann constant and ν is the frequency of observed transition. Assuming ^{12}CO (1-0) emission is optically thick ($\tau \gg 1$) and the filling factor $f=1$, the excitation temperature T_{ex} can be straightforwardly obtained. Since the Planck cold clumps are clearly extended and are mostly resolved by Planck observations (Planck Collaboration. et al. 2011), the assumption of filling factors for gas $f=1$ is reasonable.

Assuming the ^{13}CO (1-0) and C^{18}O (1-0) lines are optically thin and they have the same excitation temperature as ^{12}CO (1-0), the column density of ^{13}CO and C^{18}O under LTE condition can be obtained as following (Garden et al. 1991; Pillai et al. 2007):

$$N_{total} = \frac{3h\varepsilon_0}{2\pi^2 S \mu_g^2} \frac{J(T_{ex}) Q(T_{ex}) W}{J_\nu(T_{ex}) - J_\nu(T_{bg})} \quad (2)$$

where ε_0 is the dielectric permittivity, $S \mu_g^2$ is the line strength multiplied by the dipole moment along the molecular g -axis. $J(T_{ex})$ is defined as (Pillai et al. 2007)

$$J(T_{ex}) = \frac{\exp(E_u/kT_{ex})}{\exp(h\nu/kT_{ex}) - 1} \quad (3)$$

where E_u is the upper energy level. $J_\nu(T)$ is defined as (Pillai et al. 2007)

$$J(T) = \frac{h\nu/k}{\exp(h\nu/kT) - 1} \quad (4)$$

where $T_{bg} = 2.73$ is the temperature of the cosmic background radiation.

Then we calculated the peak optical depth τ_0 of ^{13}CO (1-0) and C^{18}O (1-0) from equation (1) and applied a correction factor $C_{\tau-LTE} = \frac{\tau_0}{1-\exp(-\tau_0)}$ to the column density. The correction factor obtained using peak optical depth is usually larger than the correction factor obtained using integrals of functions of the optical depth over velocity (Pineda et al. 2010). The difference is especially substantial at high optical depth (Pineda et al. 2010). However, the median peak optical depth of the C^{18}O (1-0) lines is 0.2 and the ^{13}CO (1-0) lines without corresponding C^{18}O (1-0) emission is 0.5, indicating this problem with the opacity correction is not serious here.

The LTE assumption is another crucial factor of the uncertainties in determining the column density. In non-LTE case, the excitation temperature of the ^{13}CO (1-0) and C^{18}O (1-0) lines may be very different from that of ^{12}CO (1-0) (Liu et al. 2012a). We applied RADEX (van der Tak et al. 2007), a one-dimensional non-LTE radiative transfer code, to investigate the effect of non-LTE on the determination of column density of ^{13}CO . The median value of ^{13}CO column density under LTE assumption is $3.7 \times 10^{15} \text{ cm}^{-2}$. The median values of the linewidth of ^{13}CO (1-0) and ^{12}CO (1-0) are 1.1 and 1.8 km s^{-1} , respectively. We fix the volume density of H_2 as $2.0 \times 10^3 \text{ cm}^{-3}$, which is the mean value of the whole C3PO sample (Planck Collaboration. et al. 2011). Taking the typical values mentioned above and assuming that the relative abundance of ^{12}CO to ^{13}CO is 65, we simulated the emission of ^{12}CO (1-0) and ^{13}CO (1-0) in a parameter space for the kinetic temperature of [5,20] K using LVG model in RADEX.

In the left panel of Figure 1, we plot the excitation temperature of ^{12}CO (1-0) and the ratio of the excitation temperature of ^{12}CO (1-0) T_{ex}^{12} to that of ^{13}CO (1-0) T_{ex}^{13} as a function of the kinetic temperature T_k . There is a linear relation between the the excitation temperature of ^{12}CO (1-0) and the kinetic temperature: $T_{ex}^{12} = 0.89 \times T_k + 0.73$. The ratio of T_{ex}^{12} to T_{ex}^{13} ranges from 1.13 to

1.26 with a mean value of 1.22, indicating that the LTE assumption overestimates the excitation temperature of ^{13}CO (1-0) by a factor of $\sim 20\%$. This leads to an underestimation of the ^{13}CO (1-0) opacity which in turn affects the opacity correction of the column density. From the right panel of Figure 1, one can see that the optical depth of ^{12}CO (1-0) decreases with the kinetic temperature but is much larger than 1. The optical depth of ^{13}CO (1-0) calculated with RADEX also decreases with the kinetic temperature. At low kinetic temperature ($T_k < 8$ K), the ^{13}CO (1-0) emission may become optically thick. We also noticed that the optical depth of ^{13}CO (1-0) calculated with RADEX is larger than that calculated under LTE assumption, especially at low kinetic temperatures. Therefore the opacity correction factor C_τ under non-LTE condition should be larger than $C_{\tau-LTE}$. However, the overestimation of the excitation temperature not only affect the optical depth but also affect the partition function. The partial function Z is given by

$$Z = \sum_{J=0}^{\infty} (2J+1) e^{\frac{-hB(J+1)}{kT_{ex}}} \approx \frac{kT_{ex}}{hB}, \text{ when } T_{ex} \gg hB/k. \quad (5)$$

Thus the correction factor on Z due to non-LTE can be defined as $C_Z = \frac{Z_{non-LTE}}{Z_{LTE}} = \frac{T_{ex}^{13}}{T_{ex}^{12}}$. Where T_{ex}^{13} and T_{ex}^{12} are the excitation temperatures of ^{13}CO (1-0) and ^{12}CO (1-0), respectively. In the right panel of Figure 1, we plot C_Z and $C_\tau C_Z / C_{\tau-LTE}$ as function of T_{ex}^{12} . We find that C_Z is smaller than 1. $C_\tau C_Z / C_{\tau-LTE}$ is larger than 1 at lower temperature end, while smaller than 1 at high temperature end. However, $C_\tau C_Z / C_{\tau-LTE}$ varies slightly around 1 by a factor less than 20%, indicating that the uncertainty in the estimation of column density due to non-LTE effect is less than 20%. For this reason, we use the column density estimated under LTE assumption in the following analysis.

The total column density of H_2 (N_{H_2}) can be calculated with (Planck Collaboration. et al. 2011)

$$N_{\text{H}_2} = \frac{S_\nu}{\Omega_c \kappa_\nu B_\nu(T) \mu m_H} \quad (6)$$

where S_ν is the flux density at 857 GHz integrated over the solid angle $\Omega_c = \frac{\pi}{4} \sigma_{Maj} \sigma_{Min}$ with σ_{Maj} and σ_{Min} the major and minor axis of the source, $B_\nu(T)$ is the Planck function at temperature T , $\mu = 2.33$ is the mean molecular weight, and m_H is the mass of atomic hydrogen. The dust opacity

$\kappa_\nu = 0.1(\nu/1 \text{ THz})^\beta \text{ cm}^2\text{g}^{-1}$, with β the dust emissivity spectral index (Planck Collaboration. et al. 2011).

The mass of the clumps are calculated as (Planck Collaboration. et al. 2011)

$$M = \frac{S_\nu D^2}{\kappa_\nu B_\nu(T)} \quad (7)$$

where S_ν is the integrated flux density at 857 GHz, D is the distance.

The Bolometric luminosity is defined by (Planck Collaboration. et al. 2011)

$$L = 4\pi D^2 \int_\nu S_\nu d\nu \quad (8)$$

where S_ν is the flux density at frequency ν . The bolometric luminosity, L , is integrated over the frequency range $300 \text{ GHz} < \nu < 10 \text{ THz}$, using the modelled SEDs (Planck Collaboration. et al. 2011). The luminosity-to-mass ratio of the clumps ranges from 9×10^{-3} to $3.5 L_\odot/M_\odot$, with a median value of $0.2 L_\odot/M_\odot$, indicating the Planck cold clumps are not significantly affected by star forming activities.

The averaged volume density is defined by

$$n_{H_2} = N_{H_2}/\sigma_{Min} \quad (9)$$

The resulting volume density ranges from $\sim 10^2$ to $\sim 10^5 \text{ cm}^{-3}$, with a mean value of $5.4 \times 10^3 \text{ cm}^{-3}$, which is slightly larger than the mean value ($2 \times 10^3 \text{ cm}^{-3}$) of the whole C3PO sample (Planck Collaboration. et al. 2011).

If ^{12}CO (1-0) emission has corresponding C^{18}O (1-0) emission, the column density of ^{12}CO ($N_{^{12}\text{CO}}$) is converted from $N_{^{18}\text{CO}}$ with the $^{16}\text{O}/^{18}\text{O}$ isotope ratio as (Wilson & Rood 1994)

$$\frac{^{16}\text{O}}{^{18}\text{O}} = 58.8 \frac{R}{\text{kpc}} + 37.1 \quad (10)$$

where R is the Galactocentric distance.

Otherwise, we converted N_{13CO} to N_{12CO} using the $^{12}C/^{13}C$ isotope ratio given by (Pineda et al. 2013)

$$\frac{^{12}C}{^{13}C} = 4.7 \frac{R}{\text{kpc}} + 25.05 \quad (11)$$

The above relationship gives a $^{12}C/^{13}C$ isotope ratio of 65 at $R=8.5$ kpc.

In the sample, about ~30% clumps have double or multiple velocity components in ^{12}CO emission and ~16% have double or multiple velocity components in ^{13}CO emission (Wu et al. 2012). We only considered the velocity components having ^{13}CO emission in the calculation of the abundance. The observed ^{12}CO abundance is $[^{12}CO/H_2] = \frac{\sum_i N_{12CO}^i}{N_T}$, where i denotes the number of the ^{13}CO velocity components of each source. One should keep in mind that in the calculation we assume the dust emission is uniform in the clumps, which may be not the case because in our CO mapping survey (Liu, Wu & Zhang 2012) and Herschel follow-up surveys (Juvela et al. 2010, 2012) most of the Planck clumps have sub-structures. This insufficiency can be improved in future by comparing the CO maps with the dust emission maps obtained from higher resolution observations (e.g. Herschel or ground-based telescopes like APEX).

The median and mean values of the observed gaseous ^{12}CO abundance are 0.89×10^{-4} and 1.28×10^{-4} , respectively.

3.2. CO depletion and CO-to- H_2 conversion factor

The CO depletion factor, f_D , is defined as:

$$f_D = \frac{X_{12CO}^E}{[^{12}CO/H_2]} \quad (12)$$

where X_{12CO}^E is the 'expected' abundance of CO.

Taking into account the variation of atomic carbon and oxygen abundances with the Galactocentric distance, the expected ^{12}CO abundance at the Galactocentric distance R of each

source is (Fontani et al. 2012):

$$X_{12CO}^E = 8.5 \times 10^{-5} \exp(1.105 - 0.13R(\text{kpc})) \quad (13)$$

This relationship gives a canonical CO abundance of $\sim 8.5 \times 10^{-5}$ in the neighborhood of the solar system (Frerking, Langer & Wilson 1982; Langer et al. 1989; Pineda, Caselli & Goodman 2008).

The mean and median of CO depletion factor are 1.7 and 0.9, respectively. About 53% Planck cold clumps have CO depletion factor smaller than 1. Only $\sim 13\%$ Planck cold clumps have CO depletion factor larger than 3 and Only about 5.6% larger than 5. It seems that the CO gas in Planck cold clumps is not severely depleted. And due to the large beam size of PMO 13.7 m telescope and Planck satellite, we can not separate the depleted gas from the non-depleted gas, which should influence the interpretation of the CO depletion measurements. Thus our measurements indicate that on clump scale the CO depletion is not significant, in agreement with the fact that on such scales the observed emission arise mostly from low-density, non-depleted gas.

The CO-to-H₂ conversion factor $X_{CO-to-H_2} = \frac{N_T}{\sum_i I_{CO}^i}$, with I_{CO}^i the integrated intensity of the ¹²CO (1-0) line. The median value of $X_{CO-to-H_2}$ for the whole sample is $2.8 \times 10^{20} \text{ cm}^{-2} \text{K}^{-1} \text{km}^{-1} \text{ s}$. However, CO emission may be saturated at high column density, which will add uncertainties in measuring $X_{CO-to-H_2}$. Within the Perseus molecular cloud, the ¹²CO emission saturates at $A_V \sim 4$ mag (Pineda, Caselli & Goodman 2008). If we only consider the Planck cold clumps with $A_V < 4$ mag ($N_{H_2} < 3.8 \times 10^{21} \text{ cm}^{-2}$), the median and mean values of $X_{CO-to-H_2}$ are 1.7 and $1.9 \times 10^{20} \text{ cm}^{-2} \text{K}^{-1} \text{km}^{-1} \text{ s}$, respectively, which are in agreement with the mean value of $(1.8 \pm 0.3) \times 10^{20} \text{ cm}^{-2} \text{K}^{-1} \text{km}^{-1} \text{ s}$ for the Milky Way (Dame, Hartmann & Thaddeus 2001).

4. Discussion

4.1. The relationships between various physical parameters

In Figure 2, we investigate the relationships between CO abundance and dust temperature (T_d), dust emissivity spectral index (β), column density of H_2 (N_{H_2}), volume density of H_2 (n_{H_2}), luminosity-to-mass ratio (L/M) as well as the non-therm one dimensional velocity dispersion (σ_{NT}). CO abundance strongly correlates with T_d and L/M and anti-correlates with β , N_{H_2} and n_{H_2} . These relationships were well fitted with a power-law function ($y = \eta \cdot x^\zeta$). The coefficients of each model as well as the correlation coefficients R^2 are displayed in the upper-right corner of each panel. There is no correlation between CO abundance and σ_{NT} , indicating that turbulence has no effect on the fluctuation of CO abundance. The lower CO abundance for the clumps with lower T_d and with higher N_{H_2} or n_{H_2} indicates that CO gas may freeze out significantly towards cold and dense regions. The growth of icy mantles on dust grains could steepen the slope of the dust SED and thus increase the emissivity spectral index β (Schnee et al. 2010). The anti-correlation between CO abundance and β indicates that huge amount of gaseous CO transforms to icy CO with the growth of icy mantles on dust grains. However, the presence of observational errors makes the anti-correlation between the T_d and β become unreliable in the C3PO sample (Planck Collaboration. et al. 2011). Thus the relationships between β and the other physical parameters should be taken seriously and tested by further more detailed observations.

In Figure 3, we plot the CO depletion factor f_D as a function of T_d , β , N_{H_2} , n_{H_2} , L/M and σ_{NT} . The f_D significantly anti-correlates with T_d and L/M and positively correlates with β , N_{H_2} and n_{H_2} . These relationships were well fitted with a power-law function ($y = \eta \cdot x^\zeta$). In each panel, we divide the data into ten bins and plot median f_D in each bin as red filled circles. We find that the median f_D is larger than 1 in bins with $T_d < 10.8$ K or $\beta > 2.5$ or $N_{H_2} > 6.6 \times 10^{21}$ cm^{-2} or $n_{H_2} > 1.7 \times 10^3$ cm^{-3} or $L/M < 0.16$, indicating that CO gas freeze out in cold and dense regions without significant internal heating. There is also no correlation between CO depletion factor f_D

and σ_{NT} .

The variation of gaseous CO abundance in molecular clouds should seriously hamper its utility as an estimator of the total hydrogen column density. In Figure 4, we plot the CO-to- H_2 conversion factor $X_{CO-to-H_2}$ against T_d , β , N_{H_2} , n_{H_2} , L/M and σ_{NT} . In each panel, the median values of $X_{CO-to-H_2}$ in each bin are plotted as red filled circles. There is an inverse correlation between $X_{CO-to-H_2}$ and T_d and L/M . While $X_{CO-to-H_2}$ positively correlates to β , N_{H_2} and n_{H_2} . These relationships can be well fitted with power-law functions. There is no correlation between $X_{CO-to-H_2}$ and σ_{NT} . We found that the median value of $X_{CO-to-H_2}$ is larger than $2 \times 10^{20} \text{ cm}^{-2} \text{ K}^{-1} \text{ km}^{-1} \text{ s}$ in bins with $T_d < 12 \text{ K}$ or $\beta > 2.4$ or $N_{H_2} > 2.6 \times 10^{21} \text{ cm}^{-2}$ or $n_{H_2} > 2.8 \times 10^2 \text{ cm}^{-3}$ or $L/M < 0.34$.

4.2. Gaseous CO abundance — An evolutionary tracer for molecular clouds

The freezing out of gaseous CO onto grain surfaces strongly influences the physical and chemical properties of molecular clouds. As a major destroyer of molecular ions, the CO depletion leads to a change in the relative abundances of major charge carriers (e.g. H_3^+ , N_2H^+ and HCO^+) and thus causes variation in the ionizing degree (Caselli et al. 1999; Bergin & Tafalla 2007). Another second-effect induced by CO depletion is deuterium enrichments in cold cores (Caselli et al. 1999; Bergin & Tafalla 2007). These effects make gaseous CO abundance a promising tool to time the evolution of molecular clouds. As discussed in section 1, significant fraction of CO molecules is transformed from gas to solid as the gas density increases (Hernandez et al. 2011; Whittet, Goldsmith & Pineda 2010). As molecular clump evolves, the density and temperature increase. The bolometric luminosity also increases as the protostars form and evolve in molecular clumps (Emprechtinger et al. 2009). The ratio of bolometric luminosity to submillimeter emission is also used as an effective indicator for protostar evolution. In this work, we found that the relative abundance of gaseous CO significantly anti-correlates with dust temperature

and luminosity-to-mass ratio and positively correlates with column density, volume density and dust emissivity spectral index, indicating that gaseous CO abundance can also well serve as an evolutionary indicator.

One should keep in mind that the Planck cold clumps are cold (< 14 K) (Planck Collaboration. et al. 2011), turbulence dominated and have relatively low column densities comparing with the other star forming regions (Wu et al. 2012). They are mostly quiescent and lacking star forming activities, indicating that the Planck cold clumps are most likely at the very initial evolutionary stages of molecular clouds (Wu et al. 2012). Thus the relationships between various physical parameters reported here may be only valid for molecular clouds without significant star forming activities. However, our results indicate that gaseous CO abundance (or depletion) can be used as a tracer for the evolution of molecular clouds. Actually, people have already used CO depletion to distinguish relatively evolved starless cores from more-recently condensed cores (Tafalla & Santiago 2004; Tafalla 2010).

Acknowledgment

We are grateful to the staff in the Qinghai Station of Purple Mountain Observatory. Thanks for the Key Laboratory for Radio Astronomy, CAS for partly support the telescope operating. This work was funded by China Ministry of Science and Technology under State Key Development Program for Basic Research 2012CB821800 and by the National Natural Science Foundation of China under Grant No.11073003 and 11233004. Many thanks to the anonymous referee for his/her useful suggestions and comments.

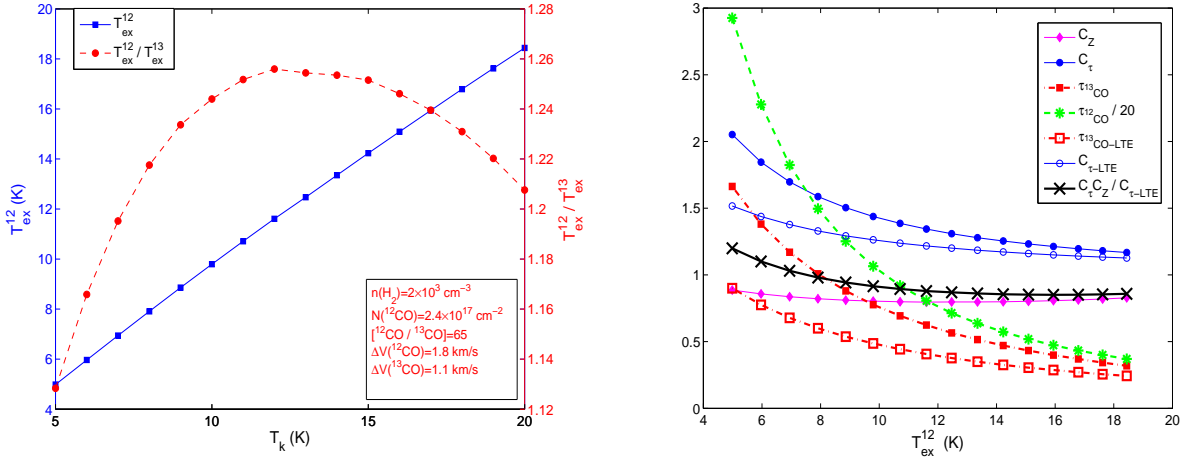


Fig. 1.— Left: T_{ex}^{12} and T_{ex}^{12}/T_{ex}^{13} as a function of T_k in the simulation with RADEX. Right: Optical depth and correction factors (see section 3.1) from RADEX simulation.

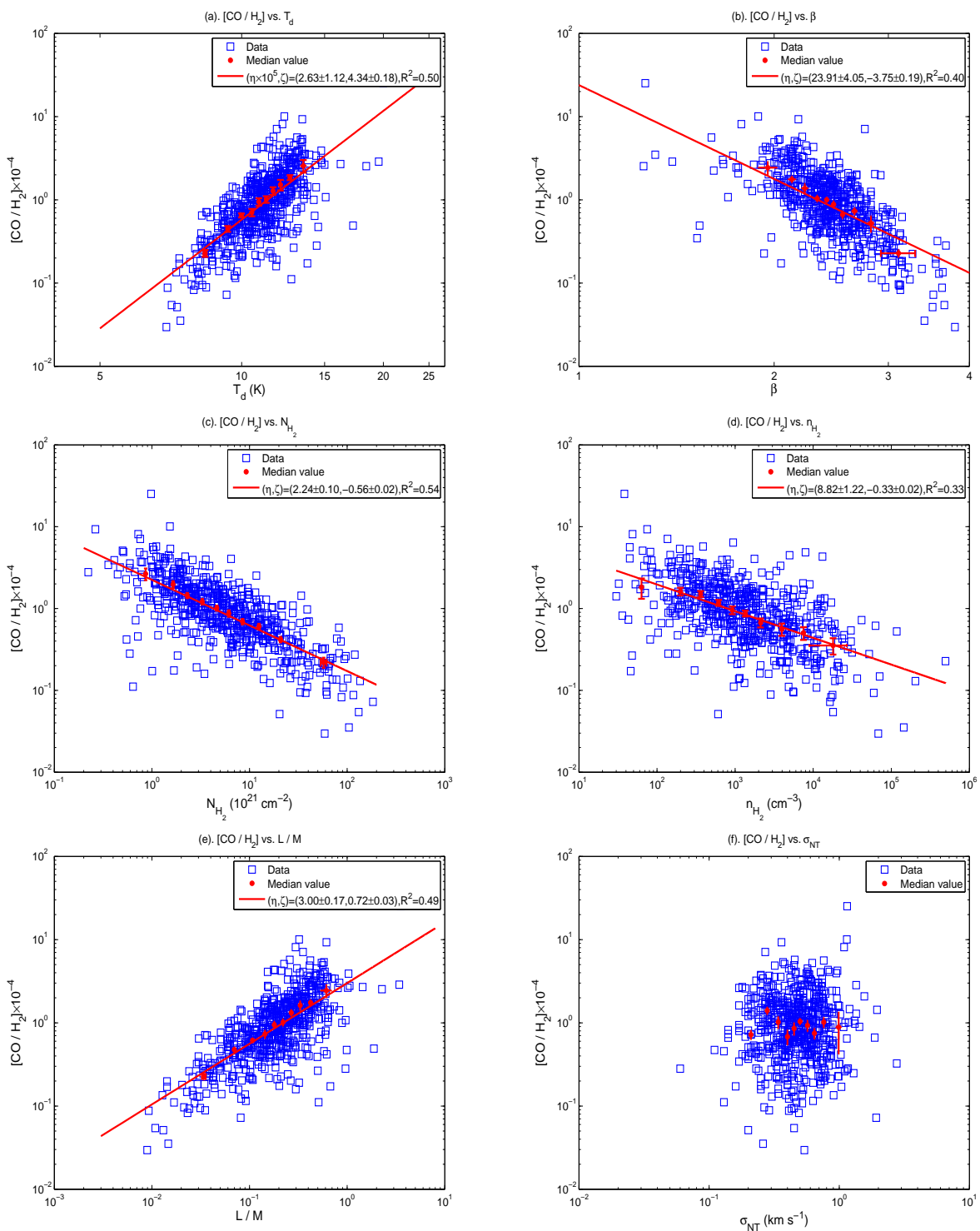


Fig. 2.— The CO relative abundance $[\text{CO}/\text{H}_2]$ as a function of T_d (a), β (b), N_{H_2} (c), n_{H_2} (d), L/M (e) and σ_{NT} (f). The red line in each panel (also in Figure 3 and 4) is power-law fitting. In each panel (also in Figure 3 and 4), the red filled circles represent the median value in each bin and the size of the green error bars represent the standard error.

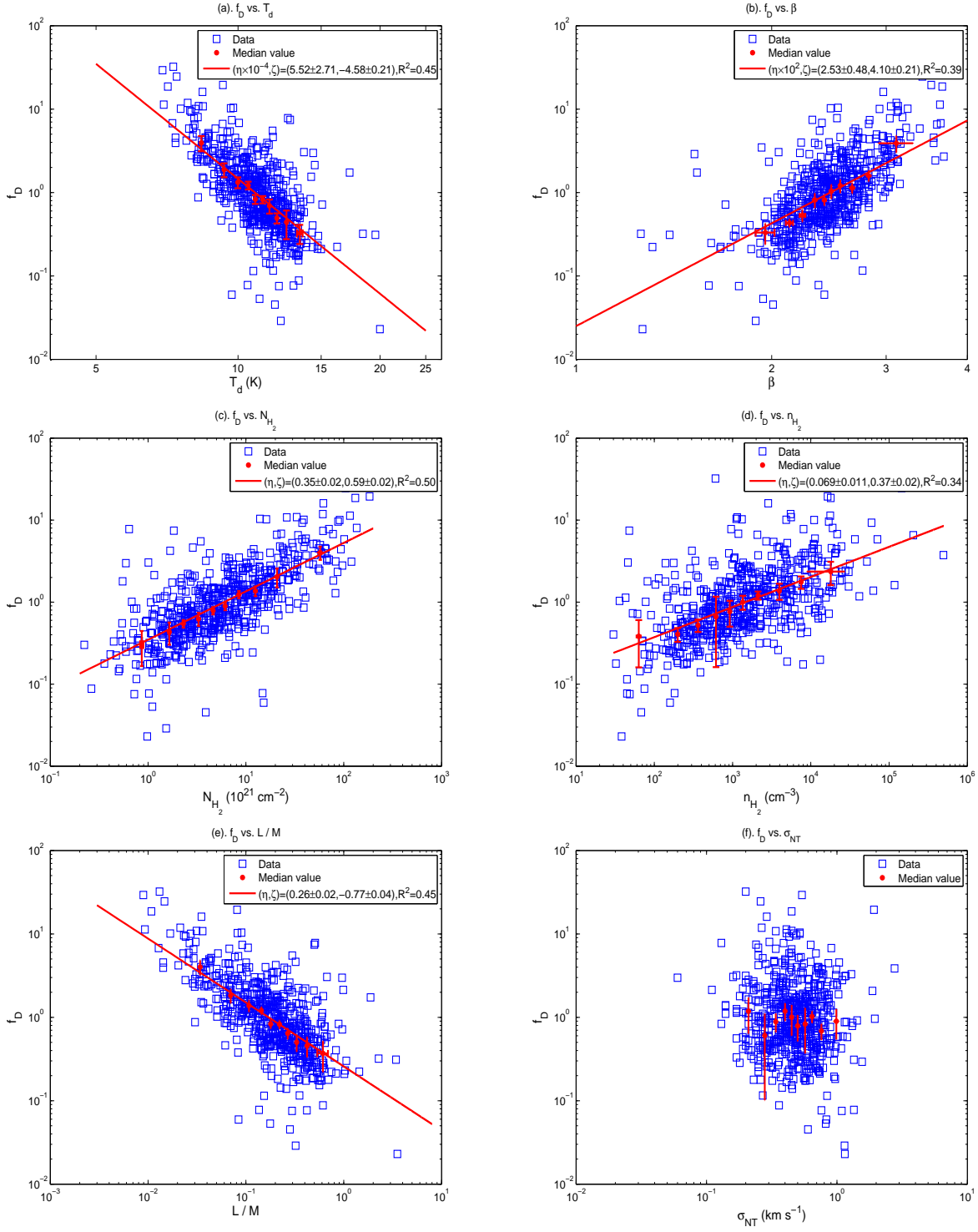


Fig. 3.— The CO depletion factor f_D as a function of T_d (a), β (b), N_{H_2} (c), n_{H_2} (d), L/M (e) and σ_{NT} (f). Other signs are the same as in Figure 2.

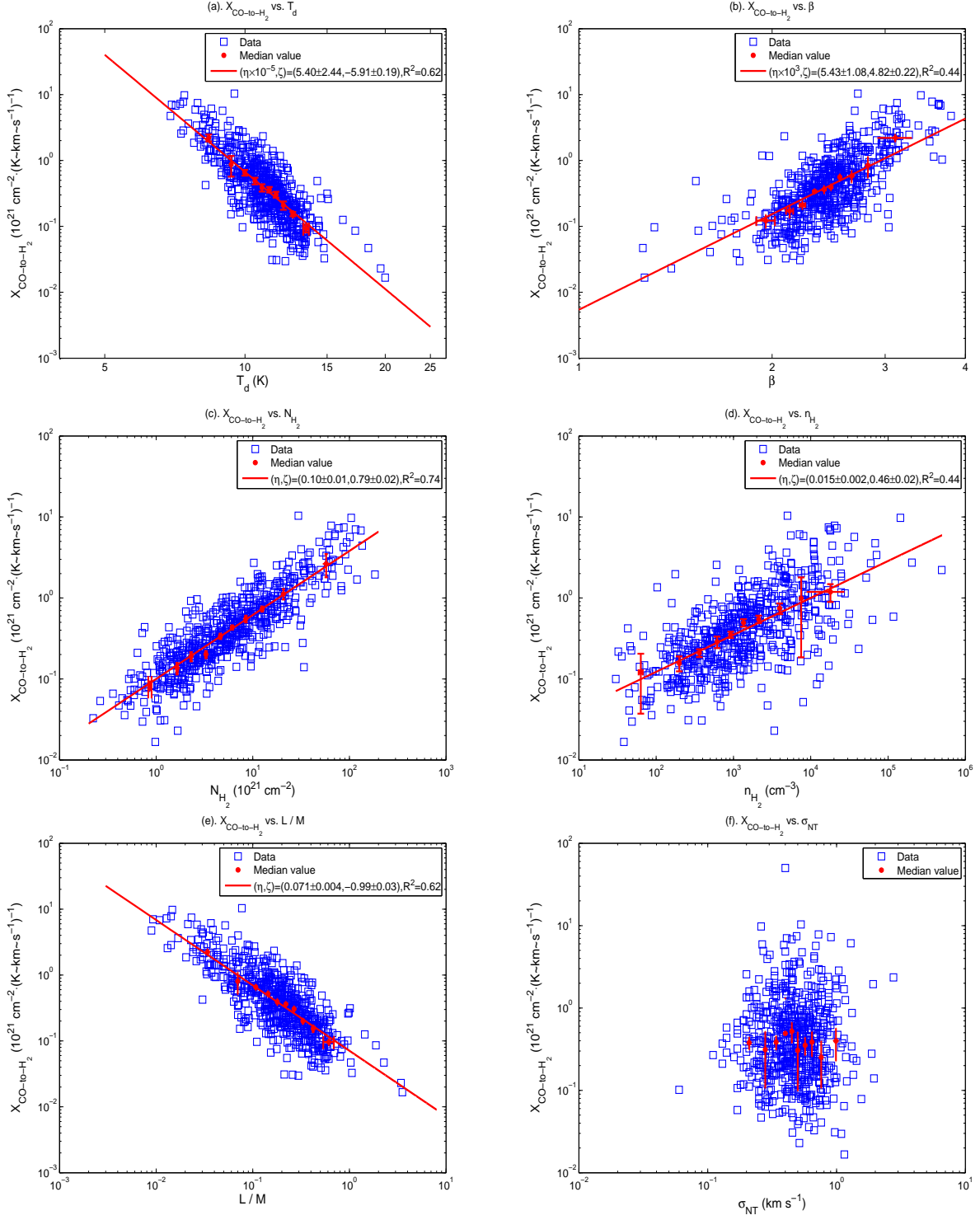


Fig. 4.— The CO-to-H₂ conversion factor $X_{\text{CO-to-H}_2}$ as a function of T_d (a), β (b), N_{H_2} (c), n_{H_2} (d), L/M (e) and σ_{NT} (f). Other signs are the same as in Figure 2.

REFERENCES

- Bergin, E. A. & Tafalla, M., 2007, *ARA&A*, 45, 339
- Caselli, P., Walmsley, C. M., Tafalla, M., Dore, L., Myers, P. C., 1999, *ApJ*, 523, L165
- Christie, H., Viti, S., Yates, J., Hatchell, J., Fuller, G. A. et al., 2012, *MNRAS*, 422, 968
- Dame, T. M., Hartmann, D., & Thaddeus, P. 2001, *ApJ*, 547, 792
- Emprechtinger, M., Caselli, P., Volgenau, N. H., Stutzki, J., & Wiedner, M. C., 2009, *A&A*, 493, 89
- Fontani, F., Giannetti, A., Beltrán, M. T., Dodson, R., Rioja, M., Brand, J., Caselli, P., Cesaroni, R., 2012, *MNRAS*, 423, 2342
- Frerking, M., Langer, L., Wilson, R. 1982, *ApJ*, 262, 590
- Garden, R. P., Hayashi, M., Hasegawa, T., Gatley, I., Kaifu, N., 1991, *ApJ*, 374, 540
- Hernandez, A. K., Tan, J. C., Caselli, P., Butler, M. J., Jiménez-Serra, I., Fontani, F., Barnes, P., 2011, *ApJ*, 738, 11
- Juvela, M., Ristorcelli, I., Montier, L. A., et al. 2010, *A&A*, 518, L93
- Juvela, M., Ristorcelli, I., Pagani, L., et al. 2012, *A&A*, 541, A12
- Kramer, C., Alves, J., Lada, C. J., Lada, E. A., Sievers, A., Ungerechts, H., & Walmsley, C. M. 1999, *A&A*, 342, 257
- Langer, W. D., Wilson, R. W., Goldsmith, P. F., & Beichman, C. A. 1989, *ApJ*, 337, 355
- Liu, T., Wu, Y., Zhang, H., Qin, S.-L., 2012a, *ApJ*, 751, 68
- Liu, T., Wu, Y., Zhang, H., 2012b, *ApJS*, 202, 4
- Pillai, T., Wyrowski, F., Hatchell, J., Gibb, A. G. & Thompson, M. A., 2007, *A&A*, 467, 207

- Pineda, J. E., Caselli, P. & Goodman, A. A., 2008, *ApJ*, 679, 481
- Pineda, J. L., Goldsmith, P. F., Chapman, N., Snell, R. L., Li, D., Cambr esy, L., Brunt, C. 2010, *ApJ*, 721, 686
- Pineda, J. L., Langer, W. D., Velusamy, T., Goldsmith, P. F., 2013, accepted to *A&A*, arXiv:1304.7770
- Planck Collaboration., Ade, P. A. R., Aghanim, N., Arnaud, M., Ashdown, M., et al., 2011, *A&A*, 536, 23
- Rodr guez, L. F., Carral, P., Moran, J. M., & Ho, P. T. P. 1982, *ApJ*, 260, 635
- Schnee, S., Enoch, M., Noriega-Crespo, A., Sayers, J., Terebey, S., et al. 2010, *ApJ*, 708, 127
- Tafalla, M., Myers, P. C., Caselli, P., Walmsley, C. M., Comito, C., 2002, *ApJ*, 569, 815
- Tafalla, M., & Santiago, J. 2004, *A&A*, 414, L53
- Tafalla, M., Highlights of Spanish Astrophysics VI, Proceedings of the IX Scientific Meeting of the Spanish Astronomical Society (SEA), held in Madrid, September 13-17, 2010, Eds.: M. R. Zapatero Osorio, J. Gorgas, J. Matz Apell niz, J. R. Pardo, and A. Gil de Paz., p. 442-453
- van der Tak, F.F.S., Black, J.H., Sch oier, F.L., Jansen, D.J., van Dishoeck, E.F. 2007, *A&A*, 468, 627
- Wilson, T. L., & Rood, R. T. 1994, *ARA&A*, 32, 191
- Whittet, D. C. B., Goldsmith, P. F., & Pineda, J. L., 2010, *ApJ*, 720, 259
- Wu, Y., Wei, Y., Zhao, M., Shi, Y., Yu, W., Qin, S., Huang, M., 2004, *A&A*, 426, 503
- Wu, Y., Liu, T., Meng, F., Li, D., Qin, S.-L., Ju, B.-G., 2012, *ApJ*, 756, 76